INTERNATIONAL JOURNAL OF HYDROGEN ENERGY 37 (2012) 18547–18555

Available online at www.sciencedirect.com

SciVerse ScienceDirect

journal homepage: www.elsevier.com/locate/he

PdAgAu alloy with high resistance to corrosion by H_2S

Fernando Braun [a], *James B. Miller* [b,c], *Andrew J. Gellman* [b,c], *Ana M. Tarditi* [a], *Benoit Fleutot* [b], *Petro Kondratyuk* [b,c], *Laura M. Cornaglia* [a,*]

[a] *Instituto de Investigaciones en Catálisis y Petroquímica (FIQ, UNL-CONICET), Santiago del Estero 2829, 3000 Santa Fe, Argentina*
[b] *Department of Chemical Engineering, Carnegie Mellon University, Pittsburgh, PA 15213, USA*
[c] *National Energy Technology Laboratory, United States Department of Energy, Pittsburgh, PA 15236, USA*

ARTICLE INFO

Article history:
Received 25 June 2012
Received in revised form
4 September 2012
Accepted 7 September 2012
Available online 30 September 2012

Keywords:
PdAgAu alloy
Sulfur tolerance
Ternary alloy
Hydrogen separation membrane

ABSTRACT

PdAgAu alloy films were prepared on porous stainless steel supports by sequential electroless deposition. Two specific compositions, $Pd_{83}Ag_2Au_{15}$ and $Pd_{74}Ag_{14}Au_{12}$, were studied for their sulfur tolerance. The alloys and a reference Pd foil were exposed to $1000 H_2S/H_2$ at 623 K for periods of 3 and 30 h. The microstructure, morphology and bulk composition of both non-exposed and H_2S-exposed samples were characterized by X-ray diffraction (XRD), scanning electron microscopy (SEM) and energy-dispersive X-ray spectroscopy (EDS). XRD and SEM analysis revealed time-dependent growth of a bulk Pd_4S phase on the Pd foil during H_2S exposure. In contrast, the PdAgAu ternary alloys displayed the same FCC structure before and after H_2S exposure. In agreement with the XRD and SEM results, sulfur was not detected in the bulk of either ternary alloy samples by EDS, even after 30 h of H_2S exposure. X-ray photoelectron spectroscopy (XPS) depth profiles were acquired for both PdAgAu alloys after 3 and 30 h of exposure to characterize sulfur contamination near their surfaces. Very low S 2p and S 2s XPS signals were observed at the top-surfaces of the PdAgAu alloys, and those signals disappeared before the etch depth reached ~10 nm, even for samples exposed to H_2S for 30 h. The depth profile analyses also revealed silver and gold segregation to the surface of the alloys; preferential location of Au on the alloys surface may be related to their resistance to bulk sulfide formation. In preliminary tests, a PdAgAu alloy membrane displayed higher initial H_2 permeability than a similarly prepared pure Pd sample and, consistent with resistance to bulk sulfide formation, lower permeability loss in H_2S than pure Pd.

1. Introduction

Hydrogen has received significant attention as an energy carrier because it can be used for electricity generation in fuel cells without emission of CO_2. H_2 production from fossil fuels will continue for many decades to come because of the relatively low cost and high availability of coal and, to an increasing extent, natural gas. Conventional H_2 production from fossil-derived syngas requires multiple stages of purification to completely remove impurities such as CO and H_2S, which can deactivate the platinum electrodes of polymer electrolyte membrane fuel cells.

One strategy for reducing production costs and increasing the yield of ultrapure hydrogen is to use membrane type reactors for reforming and/or water-gas shift. In a single unit operation, membrane reactors deliver high purity hydrogen

* *Corresponding author*. Tel.: +54 342 4536861.
E-mail address: lmcornag@fiq.unl.edu.ar (L.M. Cornaglia).
0360-3199/$ – see front matter
http://dx.doi.org/10.1016/j.ijhydene.2012.09.040

Table 1 – Chemical composition of Pd, Ag and Au electroless plating solutions, activation and plating conditions.

	Activation/pH modifier	Plating bath		
		Pd	Ag	Au
$SnCl_2$ (g/l)	1	–	–	–
$PdCl_2$ (g/l)	0.10	–	–	–
HCl (M)	1	–	–	–
Hydrazine (mM)		10	10	–
28–30% NH_4OH (M)	–	9.8	9.8	–
Na_2EDTA (g/l)	–	180	180	–
$PdCl_2$ (mM)	–	20.3	–	–
$AgNO_3$ (mM)	–	–	10	–
$Na_2S_2O_3 \cdot 5H_2O$ (mM)	–	–	–	149.9
Na_2SO_3 (mM)	–	–	–	169.9
$C_6H_8O_6$ (mM)	–	–	–	339.9
$AuCl_3 \cdot HCl \cdot 4H_2O$	–	–	–	6.9
pH	–	11.5	11.5	11.0
Temperature (°C)	–	50	50	30

(by permeation of product hydrogen through reactor walls) and a separate concentrated CO_2 stream that can be sequestered. Pd-based membranes have been extensively studied for the H_2 separation application. The Pd surface is active for dissociation of molecular hydrogen and H-atoms readily diffuse through bulk Pd, enabling high selectivity for hydrogen permeation [1–6]. However, exposure to H_2S, a common minor component of methane and fossil-derived syngas, can compromise membrane permeability by formation of surface or bulk sulfides [7].

Exposure of pure Pd to H_2S is well known to cause formation of a bulk sulfide corrosion product over a wide range of H_2S concentrations (3.5–1000 ppm) and exposure temperatures (623–1100 K). The corrosion product, Pd_4S, has a hydrogen permeability about an order of magnitude lower than Pd [7,8]. To improve its tolerance to sulfur, Pd has been alloyed with various minor components [5,9–15]. PdCu has been extensively studied for its sulfur tolerance over a range of temperatures and H_2S concentrations [13,16,17]. The potential for bulk corrosion of a PdCu alloy by H_2S exposure depends not only on the alloy composition, but also on the temperature of exposure and the composition of the exposure gas; PdCu alloys will not corrode at conditions at which the sulfide corrosion product is unstable [13]. Thus, at high temperatures (generally $>$ 900 K), PdCu alloys with 30–50% Cu are completely inert to H_2S, even at concentrations of H_2S as high as 1000 ppm [13]. At lower temperatures, which are preferred for H_2 production, surface sulfides are formed, which make the surface inactive for the dissociation step [13,16,17].

PdAu has also been studied for its sulfur tolerance, but not to the same extent as PdCu [10,14,15]. Sulfide formation has been reported in low-Au composition alloys (4–7%) at mild exposure conditions (673 K and 20 ppm H_2S), while PdAu alloys with higher Au composition (~20%) have displayed high sulfur tolerance at 623 K, even upon exposure to 66,000 ppm of H_2S [10]. In addition, several authors have reported that the PdAu alloy has a higher permeability than PdCu alloy membranes [18–21]. In "clean" environments, PdAg alloys display higher permeability than PdAu, PdCu and even pure Pd. However, in the presence of H_2S, PdAg corrodes as quickly as Pd [5,10].

With the aim of combining the H_2S tolerance of the PdAu binary with the high permeance of the PdAg binary, we prepared ternary PdAgAu alloys by sequential electroless plating and characterized their resistance to bulk corrosion by H_2S. We exposed a pair of ternary alloys and a reference Pd sample to 1000 ppm of H_2S for periods of 3 and 30 h at 623 K. We show that, unlike the Pd reference sample, the ternary alloys do not react with H_2S to form bulk sulfide under these conditions.

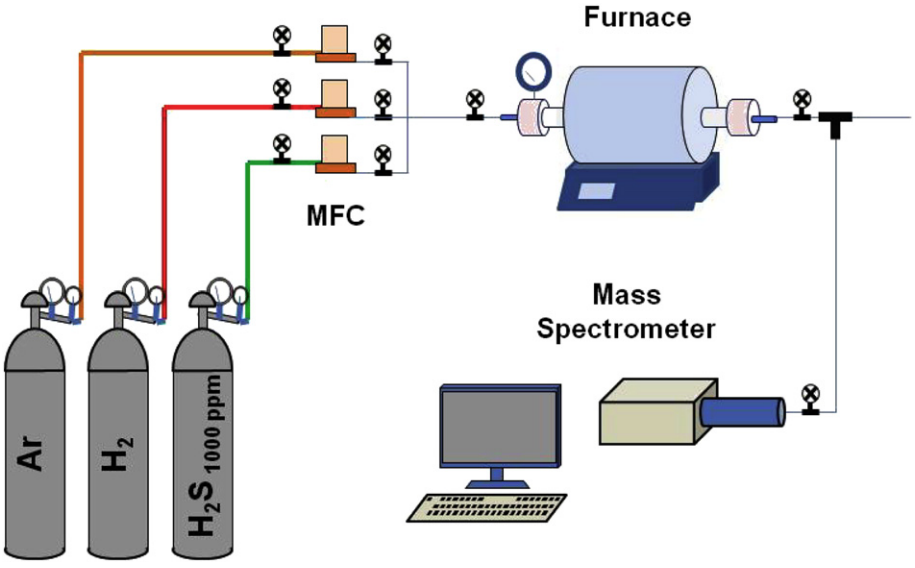

Fig. 1 – Scheme of the H_2S treatment system.

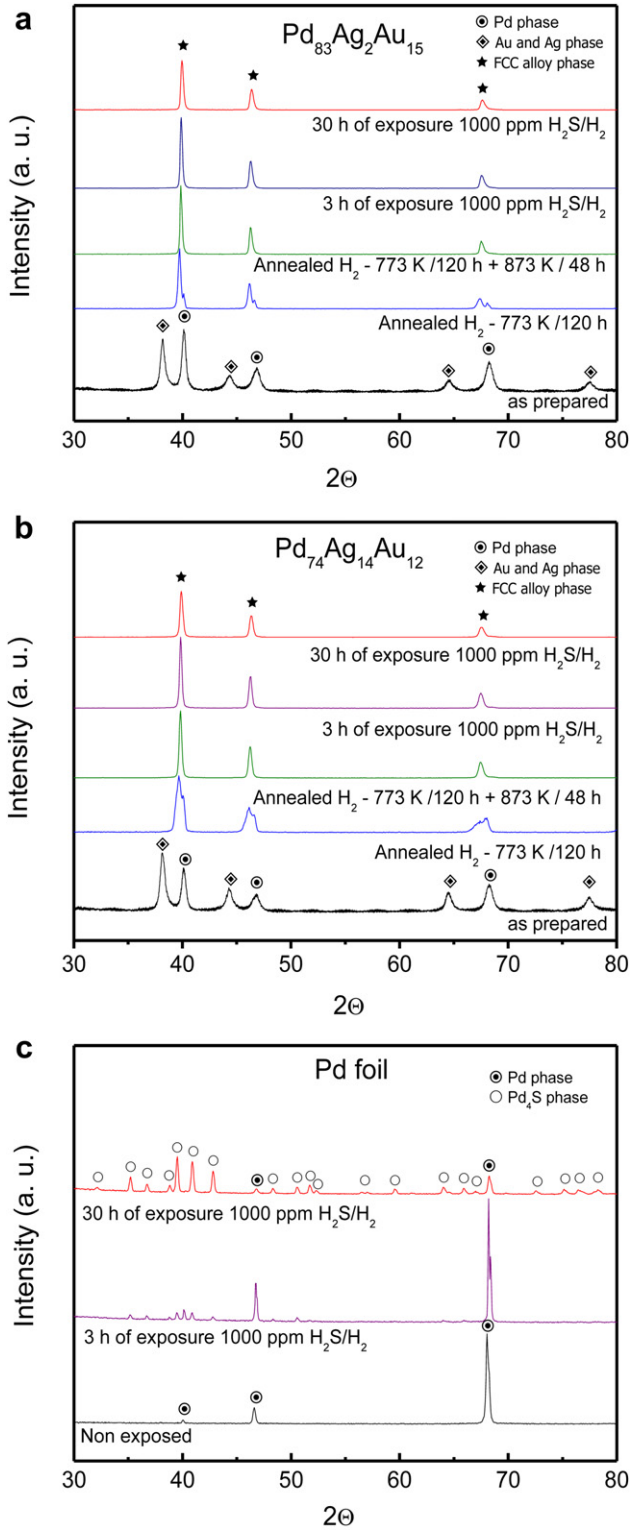

Fig. 2 – X-ray diffraction patterns of the Pd film before and after H_2S exposure (a) and both PdAgAu ternary alloys as prepared, after annealing and after H_2S exposure (b, c). Ternary samples annealing conditions: 1st cycle; 120 h at 773 K in H_2, 2nd cycle; 48 h at 873 K in H_2. H_2S treatment conditions: $T = 623$ K, $[H_2S] = 1000$ ppm, time = 3 and 30 h.

Resistance to bulk corrosion may be linked to co-segregation of Ag and especially Au to the top surface of the alloy.

2. Experimental

2.1. PdAgAu membrane preparation

Two PdAgAu films were deposited by sequential electroless plating onto porous, 0.1 μm grade (PSSD), stainless steel 316L discs, 1.27 cm diameter × 2 mm thick. Before metal deposition, discs were washed with an alkaline solution consisting of 0.12 M $Na_3PO_4 \cdot 12H_2O$, 0.6 M Na_2CO_3 and 1.12 M NaOH using the procedure reported by Ma and coworkers [22], and then annealed in air for 12 h at 773 K. To avoid intermetallic diffusion between the stainless steel substrate and the PdAgAu alloy components, the supports were modified with alumina by a vacuum assisted dip coating method [23]. Before the electroless plating step, the discs were activated. The sensitizing-activation of the substrate was performed at room temperature, first in an acidic $SnCl_2$ (1 g/l) solution, and then in an acidic $PdCl_2$ solution (0.1 g/l). The sensitizing-activation process was repeated six times. Palladium, silver and gold were deposited by sequential electroless deposition using the bath compositions shown in Table 1. For the sample with the lower Ag content, palladium was deposited in two steps of 60 min each, followed by a short Ag deposition of 5 min. In the case of the sample with the higher Ag content, palladium was deposited in two steps of 60 min and 40 min each, followed by Ag deposition for 15 min. For both samples, the Au deposition on top of the Pd–Ag layers was performed for 20 min. After the metal depositions, the samples were rinsed with water and dried at 393 K overnight. The three-metal deposition cycle was repeated for both samples to achieve a target thickness of ~ 10 μm.

The ternary samples were annealed at 773 K in H_2 to promote metallic inter-diffusion and alloy formation. The samples were mounted in a tube furnace as shown in Fig. 1 and heated from room temperature to 773 K at 0.5 K min^{-1} in flowing nitrogen. The flow was then changed to hydrogen and the samples were held at 773 K in H_2 for 120 h. X-ray diffraction experiments revealed that FCC ternary alloy formation was incomplete at 773 K, so both samples were incrementally annealed at 873 K in H_2 for 48 h.

2.2. PdAgAu membrane H_2S treatment

For the study of the sulfur tolerance of the PdAgAu alloy, two ternary alloys and a 25 μm thick Pd foil were exposed to a H_2S/H_2 gas mixture. The pure Pd foil was used as a reference because it is well known that it corrodes upon exposure to H_2S, even at low concentrations [10]. Samples of the ternary alloys and a Pd foil were mounted horizontally in a tube furnace. Then, they were heated from room temperature to 623 K at 1 K min^{-1} in a flow of high purity argon (40 ml/min). Next, the samples were treated in flowing hydrogen (10 ml/min, high purity) at 623 K for 30 min, followed by a mixture of 1000 ppm H_2S/H_2 (10 ml/min) for 3 h. Immediately after the H_2S treatment, the reactor feed gas was switched back to Ar (90 ml/min) for 25 min to sweep all the H_2S trapped in the reactor volume. After characterization, the 3-h samples were exposed to H_2S for another 27 h (for a total of 30 h of exposure).

Table 2 – Summary of literature results involving the effect of H_2S exposure to Pd, PdAg and PdAu alloys at several temperatures.

Reference	Membrane composition (Mol %)	Temperature (K)/time of exposure (h)	Feed composition	Experiment result
McKinley [10]	Pd	623/144	4.5 ppm H_2S in H_2	Dull and etched surface.
Mundschau [5]	Pd	593/120	20 ppm H_2S/60%H_2–He	Pd_4S formation.
O'Brien [16]	Pd	623/6	1000 ppm H_2S/10% He–H_2	Pd_4S formation.
This work	Pd	623/3	1000 ppm H_2S in H_2	Pd_4S formation.
Mundschau [5]	$Pd_{75}Ag_{25}$	593/65	10 ppm H_2S/80% H_2–He	Pd_4S and $Ag_5Pd_{10}S_5$ formation.
McKinley [10]	$Pd_{73}Ag_{27}$	623/48	3.5 ppm H_2S in H_2	Dull and etched surface.
McKinley [10]	$Pd_{74}Au_{26}$	623/144	4.3 ppm H_2S in H_2	Retained original luster.
McKinley [10]	$Pd_{74}Au_{26}$	623/168	20.6 ppm H_2S in H_2	Retained original luster.
McKinley [10]	$Pd_{74}Au_{26}$	623/6	66000 ppm H_2S in H_2	Retained original luster.
Gade [15]	$Pd_{94}Au_6$ (Cold-worked)	673/80	20 ppm H_2S/50%H_2/29%H_2O/19%CO_2/1%CO	Pd_4S and $Pd_{2.8}S$ formation.
Ma [14]	$Pd_{94.5}Au_{5.5}$	673/24	54.8 ppm H_2S in H_2	No bulk sulfide formation.
Coulter [28]	$Pd_{86}Au_7Pt_7$	673/100	20 ppmv H_2S/50%H_2/29%H_2O/19%CO_2/1%CO	Pd_4S formation.
This work	$Pd_{74}Ag_{14}Au_{12}$	623/30	1000 ppm H_2S in H_2	No bulk sulfide formation.
This work	$Pd_{83}Ag_2Au_{15}$	623/30	1000 ppm H_2S in H_2	No bulk sulfide formation.

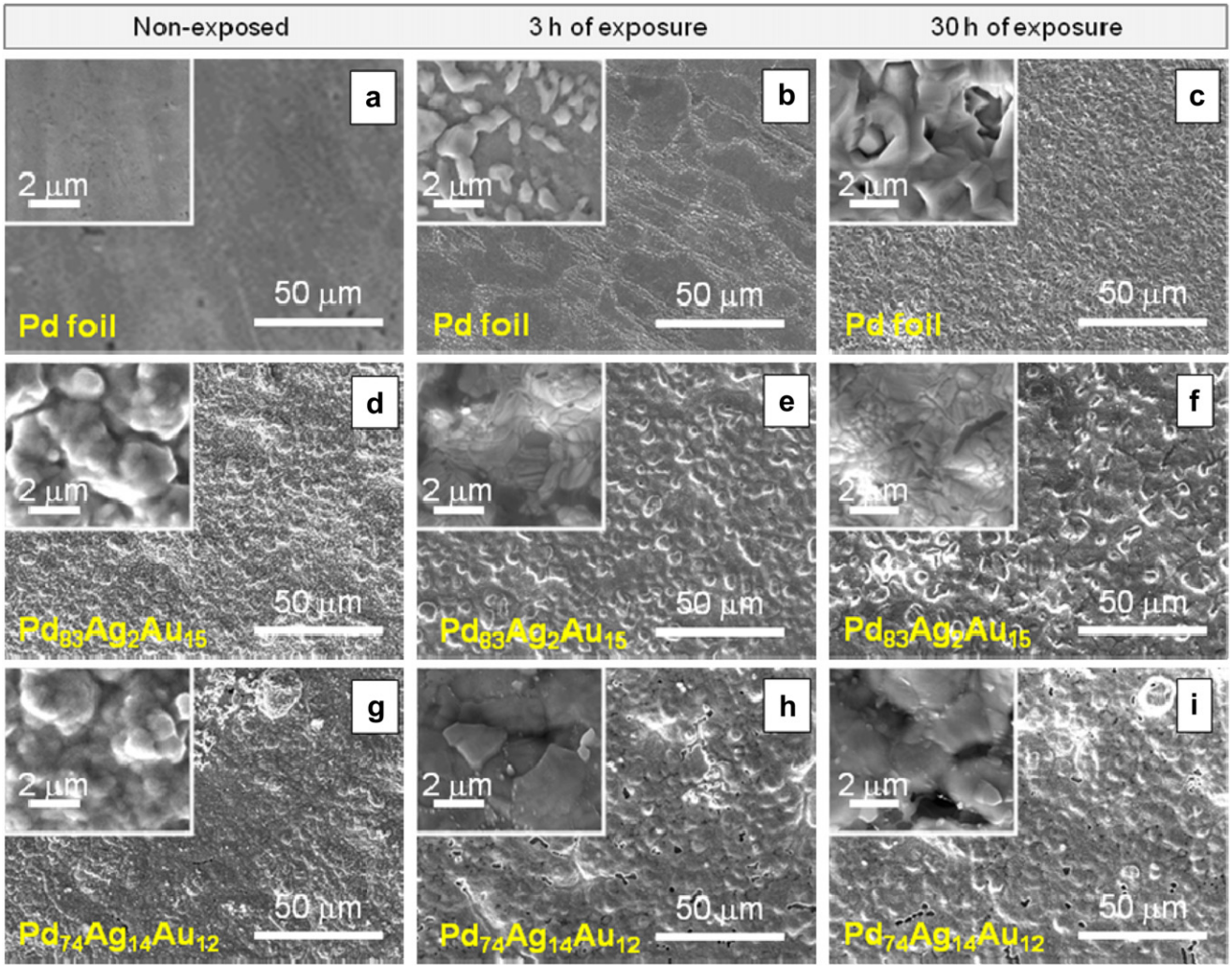

Fig. 3 – Effect of time of exposure on the morphology of Pd foil (a, b and c), $Pd_{83}Ag_2Au_{15}$ (d, e and f) and $Pd_{74}Ag_{14}Au_{12}$ (g, h and i). H_2S treatment conditions: $T = 623$ K, $[H_2S] = 1000$ ppm, time = 3 and 30 h.

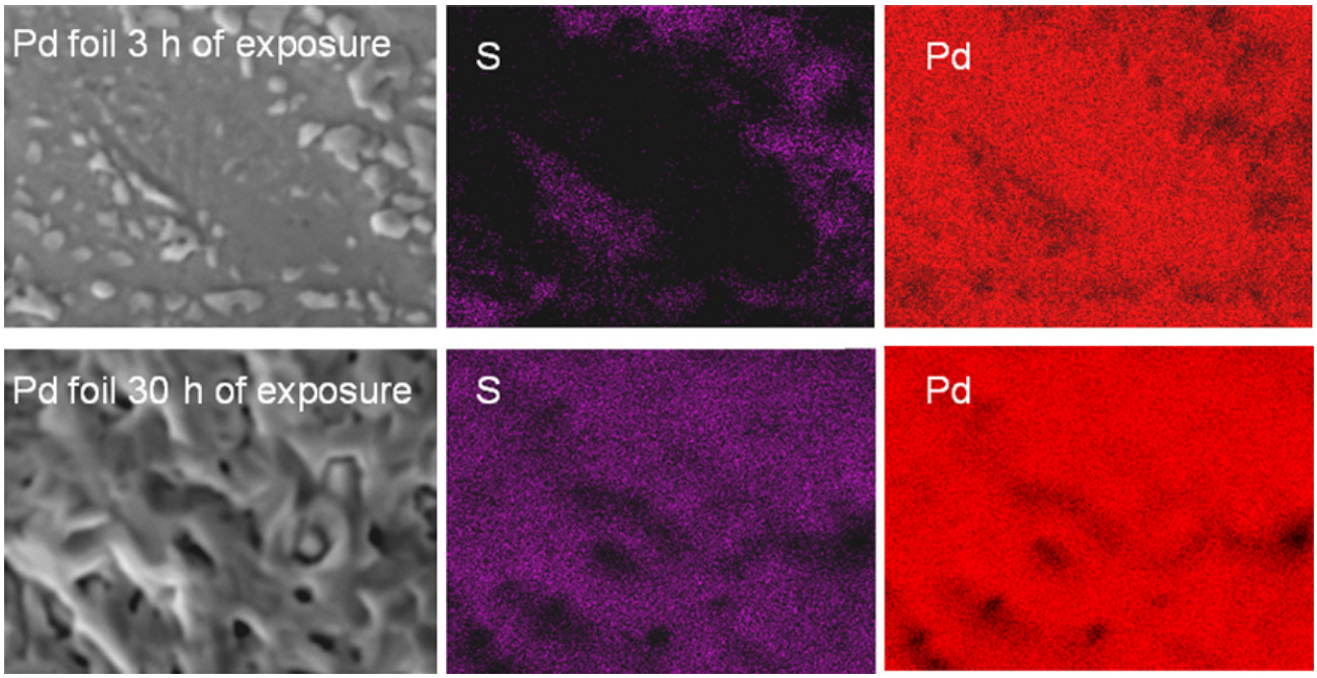

Fig. 4 – SEM surface mapping images of the Pd foil after 3 and 30 h of exposure. H_2S treatment conditions: T = 623 K, [H_2S] = 1000 ppm, time = 3 and 30 h. Color: S – Pink, Pd – red. (For interpretation of the references to color in this figure legend, the reader is referred to the web version of this article.)

2.3. *Film characterization*

2.3.1. *X-ray diffraction*

The phase structure of the samples was determined by X-ray Diffraction. The XRD patterns of the films were obtained using a PANalytical X'Pert Pro instrument, having a theta–theta configuration, a Cu X-ray source operated at 45 kV and 40 mA and an X'Celerator detector equipped with a monochromator. Patterns were recorded over a 2θ range of 20–100° at a step size of 0.02°.

2.3.2. *Scanning electron microscopy, mapping and energy-dispersive X-ray analysis*

The outer surface of the samples was imaged using a Tescan Vega-3 SEM instrument, operated at 20 kV in high-vacuum mode. The instrument was equipped with an Oxford INCA energy dispersive X-ray detection system for composition mapping; compositions were quantified using software provided by the manufacturer.

2.3.3. *Elemental depth profiles by X-ray photoelectron spectroscopy (XPS)*

XPS depth profiles were performed using a ThermoFisher Theta Probe instrument. The instrument has a base working pressure of 1.0×10^{-10} kPa; it is equipped with a monochromatic Al Kα X-ray source. The instrument's hemispherical analyzer was operated in Constant Analyzer Energy (CAE) mode with a pass energy of 200 eV. Depth profiles were performed using argon ion sputtering. A differentially pumped ion gun was operated at 1×10^{-8} kPa, 3 kV and 500 nA, conditions which delivered a sputtering rate of approximately 1 nm min^{-1}. Sputtering was performed in 10 steps of 60 s, followed by 10 steps of 180 s to examine the top ~50 nm of the sample surfaces. Before sputtering and then at each sputtering step, photoemission spectra for Pd 3d, Pd 3p, O1s, C 1s, Au 4f, S 1s, S 2p core levels were recorded; peak areas were determined by integration employing a Shirley-type background. Sensitivity factors provided by the instrument's manufacturer were used for the quantification of the elements.

3. Results and discussion

3.1. *PdAgAu alloy formation and phase analysis after exposure to H_2S*

X-ray diffraction patterns of the Pd foil and the two alloys, before and after exposure to H_2S, are displayed in Fig. 2. The XRD patterns of the as-deposited alloy samples (bottom patterns, Fig. 2a and b) contain diffraction features of a pure Pd phase ($2\theta = 40.12°, 46.62°, 68.12°$) and pure phases of Ag and Au (2θ = ~38.15°, ~44.33°, ~64.50°). After the first annealing cycle performed at 773 K during 120 h, formation of the FCC ternary alloy phase was incomplete, as illustrated by the continued appearance of small features at $2\theta = 40.12°$, 46.62° and 68.12°. For both samples, formation of the alloy FCC phase was complete after a second annealing at 873 K for 48 h.

Several investigations of PdAg and PdAu alloy formation have been reported in the literature and provide context for our results [14,24–26]. Complete formation of a $Pd_{86}Ag_{24}$FCC alloy has been observed upon annealing at 773 K in H_2 for 110 h [25]. $Pd_{93}Au_7$ alloy formation, in contrast, is a slower

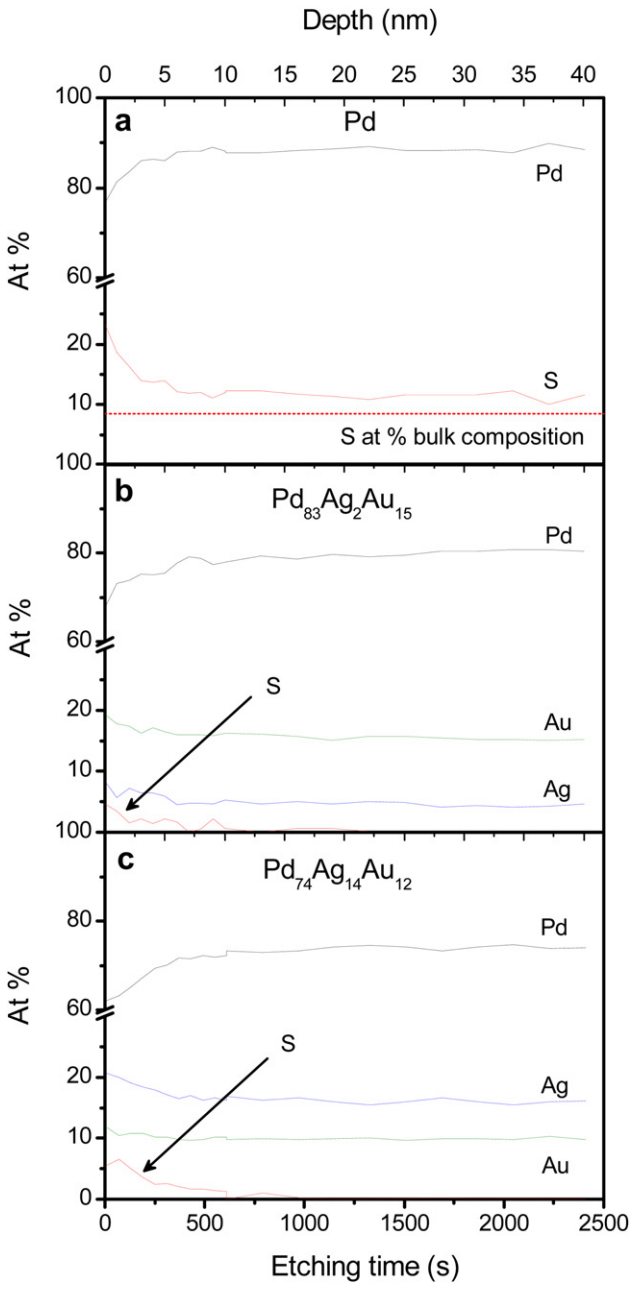

Fig. 5 – X-ray photoelectron spectroscopy depth profiles of the Pd foil (a), $Pd_{83}Ag_2Au_{15}$ (b) And $Pd_{74}Ag_{14}Au_{12}$ (c) Samples after 3 h of H_2S exposure. Elemental concentrations shown for Pd (black), Ag (blue), Au (green) and S (red). Analysis conditions: 1st 10 sputtering cycles of 60 s each. 2nd 10 sputtering cycles of 180 s each. H_2S treatment conditions: $T = 623$ K, $[H_2S] = 1000$ ppm, time = 3 h. (For interpretation of the references to color in this figure legend, the reader is referred to the web version of this article.)

process requiring more than 500 h in H_2 at 773 K [26]. The difference reflects the low solid-phase mobility of Au (Tammann temperature = 669 K) relative to Ag (Tammann temperature = 618 K). The aggressive anneal conditions that our PdAgAu alloys require for complete alloy formation suggest that the Au component dominates the alloying process.

After alloy formation, both ternary samples and a Pd foil were treated in 1000 ppm H_2S/H_2 at 623 K for 3, and then 30 h. The H_2S-exposed samples were characterized by XRD in the 30°–80° range to study the phases formed during the treatment. The Pd foil shows clear evidence of bulk sulfide growth upon H_2S exposure. A Pd_4S phase starts to form at 3 h and grows with increasing exposure time. The XRD pattern of the Pd foil exposed for 30 h (Fig. 2c) reveals an almost complete Pd_4S phase in the XRD analysis depth. In contrast, PdAgAu alloys show the same FCC phase before and after 30 h of exposure, as shown in Fig. 2a and b, with no evidence of formation of a crystalline sulfide phase.

Table 2 is a summary of results published in the literature involving the effect of H_2S exposure to Pd, PdAg and PdAu alloys at several temperatures. Several authors have used XRD to identify bulk sulfide phases in Pd and PdAg alloys upon exposure to relatively low H_2S concentrations [5,10,11,13,17,18,27]. Consistent with the results of our Pd reference sample, O'Brien et al. [16] reported complete conversion of a Pd foil to Pd_4S upon exposure to 1000 ppm H_2S at 623 K for 6 h. Mundschau et al. also observed the Pd_4S XRD pattern for a Pd foil treated with 20 ppm H_2S at 593 K for 115 h [5]. These authors also reported formation of mixed $Ag_5Pd_{10}S_5$ sulfide phase upon exposure of a $Pd_{75}Ag_{25}$ alloy membrane to 10 ppm H_2S at 593 K for 65 h.

While not studied as thoroughly as Cu, an Au minor component has also been reported to improve Pd's resistance to H_2S corrosion. Ma and co-workers [14] did not observe sulfide formation upon exposure of a $Pd_{94.5}Au_{5.5}$ alloy to 54.8 ppm H_2S in H_2 at 673 K for 24 h. McKinley reported that a $Pd_{74}Au_{26}$ alloy did not tarnish (visual inspection) upon exposure to H_2S (in H_2) concentrations as high as 6.6% at 623 K [10]. In a counter-example, formation of Pd-sulfide phases, detected by XRD, was observed in low-Au content (6–7 at%) binary and ternary alloys that were exposed to 20 ppm H_2S in a complex background of H_2, H_2O, CO_2, and CO at 673 K [15,28]; these components might have an influence on the sulfide formation. Our ternary membranes did not react to form bulk sulfides at exposure conditions more severe than those that cause corrosion of PdAg alloys, providing clear evidence of Au's role in imparting sulfur tolerance to the PdAg binary.

3.2. *Pd and PdAgAu ternary alloys morphology characterization*

The Pd foil and the ternary samples were characterized by SEM both before and after exposure to H_2S. Fig. 3 displays micrographs for the three non-exposed samples, and the same samples after 3, and then 30 h of exposure to 1000 ppm H_2S. After 3 h of exposure, the Pd foil micrograph (Fig. 3b) reveals the appearance of discrete surface aggregates, evidence of partial conversion of the foil to Pd_4S. After 30 h of treatment (Fig. 3c) the micrograph shows that the Pd_4S layer has grown to cover the entire surface. The H_2S-exposed Pd foils were also characterized by X-ray mapping, as shown in Fig. 4. The sulfur maps confirm the presence of S in the aggregates formed at 3 h, and demonstrate complete sulfur coverage after 30 h. Bulk composition characterization of the

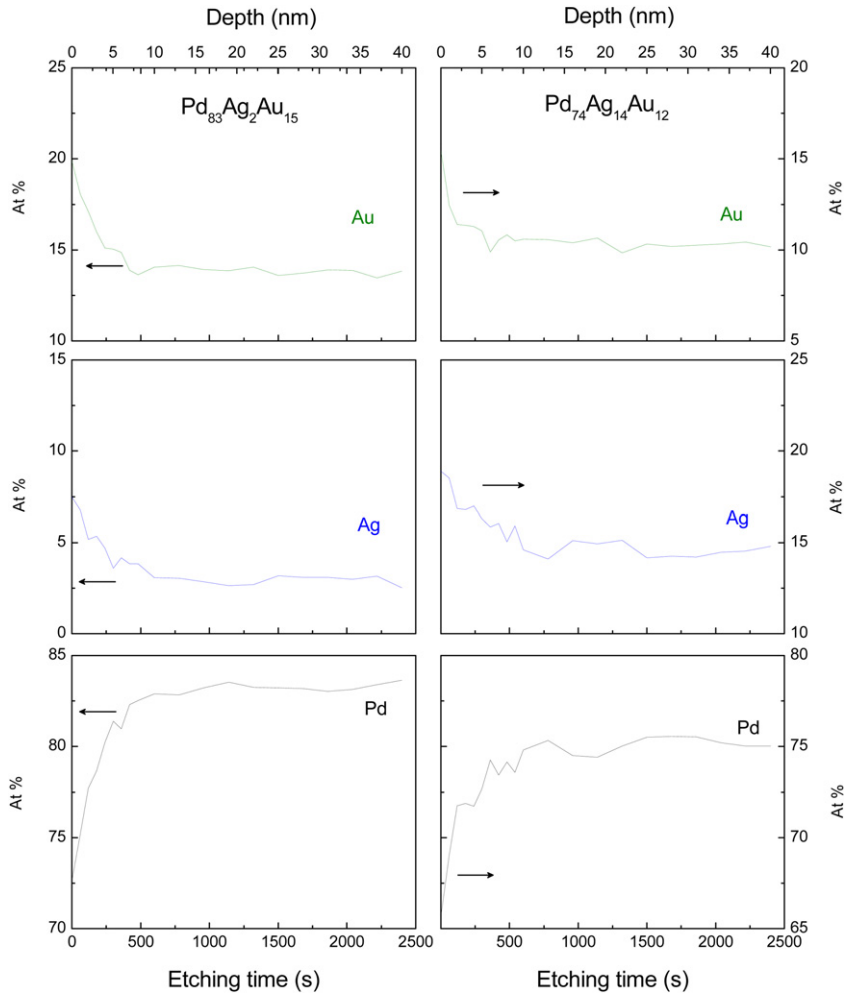

Fig. 6 – X-ray photoelectron spectroscopy depth profiles of the $Pd_{83}Ag_2Au_{15}$ (a) and $Pd_{74}Ag_{14}Au_{12}$ (b) samples after 30 h of H_2S exposure. Sulfur was not included in the Pd/Ag/Au composition. Analysis conditions: 1st 10 cycles of 60 s each. 2nd 10 cycles of 180 s each. H_2S treatment conditions: $T = 623$ K, $[H_2S] = 1000$ ppm, time = 30 h.

30-h sample by EDS revealed Pd_4S stoichiometry, confirming that the reference foil had been completely converted to the sulfide.

In contrast to the Pd foil, neither PdAgAu ternary sample exhibited a morphology change upon H_2S exposure (Fig. 2d–i). The micrograph of the $Pd_{74}Ag_{14}Au_{12}$ sample reveals pinhole pores on its surface, which is likely related to the relatively high Ag content of that sample; the dendritic morphology of the silver deposits has been reported by many authors [29,30]. EDS-mapping of the alloys after 3 and 30 h of exposure (not shown) did not reveal the presence of S. Thus, in agreement with XRD results, SEM and mapping analyses of the H_2S-exposed PdAgAu alloys did not uncover evidence of bulk sulfide formation upon aggressive treatment with H_2S.

3.3. *XPS depth profile analysis after 3 h of H_2S exposure*

To assess local sulfur contamination at the surfaces of the materials, which may be undetectable by EDS and XRD, XPS composition depth profiles were performed on the Pd foil and the ternary alloys after 3 h of H_2S exposure. The atomic compositions of Pd, Ag, Au and S as a function of etching time/depth are plotted in Fig. 5. The Pd foil has a significant sulfur content ($S > 10$ at.%) throughout the ~40 nm profiling experiment, as shown in Fig. 5a. In contrast, the depth profiles of both alloys display only very weak S signals at the top-surface (etch time = 0), which disappear before the etch depth reaches ~ 10 nm. At the same depth, the relative Pd, Ag and Au contents of the surface region reach steady state values that are the same as bulk compositions measured by EDS. Our sulfur profiles are similar to those reported by O'Brien et al. [16], who used XPS depth profiling to study the surface compositions of Pd and $Pd_{47}Cu_{53}$ foils after exposure to 1000 ppm H_2S at 623 K for 6 h. These authors observed constant sulfur content of 20 at % (i.e., Pd_4S stoichiometry) throughout the depth profile of their Pd sample. S appeared only at the very top-surface of their $Pd_{47}Cu_{53}$ alloy.

Metals composition profiles (Pd, Ag and Au only; S not included in the calculation) of the PdAgAu alloys samples after 30 h of H_2S exposure are displayed in Fig. 6. Clearly, Ag and Au co-segregate to the top surfaces (etch time = 0) of both alloys. The extent of Au segregation to the surface of $Pd_{83}Ag_2Au_{15}$

(top-surface composition: $Pd_{73}Ag_7Au_{20}$; surface/bulk Au ratio = 20/15 = 1.33) is similar to the surface of $Pd_{74}Ag_{14}Au_{12}$ sample (top-surface composition: $Pd_{66}Ag_{19}Au_{15}$; surface/bulk Au ratio = 15/12 = 1.25). Au segregation to the surface of PdAu alloys has been experimentally observed by a number of researchers [31–34]. Swartzfager et al. [31] reported a surface Au content of 52% (at.) for a $Pd_{80}Au_{20}$ alloy prepared by melting high-purity Au and Pd in a vacuum induction furnace and annealed at 873 K, while Piccolo et al. [32] reported gold concentrations of 75% and 85% in the top layers after annealing the (1 1 1) and (1 1 0) surfaces of a $Pd_{70}Au_{30}$ alloy above 723 K. Similar surface enrichment, attributed to surface segregation of Au, was observed by Goodman and co-workers [33] using 1:1 Pd-Au/Mo (110) alloy annealed at 800 K. Li et al. [34] studied the surface segregation of a Au to the surface of a Au/Pd (1 1 1) alloy by LEED and LEIS. Au and Ag enrichment at the surfaces of alloys with Pd is consistent with the pure-component surface energies: both Ag (1.2–1.4 J/m^2) and Au (1.63 J/m^2) have lower surface energies than Pd (2.05 J/m^2) [35,36]. However, further experiments would be necessary to corroborate whether the Au–Ag segregation is caused after H_2S or H_2 exposure.

As described earlier, alloying Pd with Au often improves its resistance to bulk corrosion by H_2S; the work we present here shows that Au also imparts corrosion resistance to the PdAg binary. Au preferentially segregates to the surfaces of both the PdAu binary and the PdAgAu ternary alloys; high surface concentrations of Au are likely linked to the lack of reactivity of the alloy surfaces toward H_2S. The high H_2S tolerance of the PdAgAu alloys is consistent with the Au enrichment at the surface and the pure-component standard free energies of sulfides formation at 623 K: Au_2S (−8901 J/mol), Ag_2S (−63,427 J/mol) and Pd_4S (−132,005 J/mol) [37–39].

3.4. *PdAgAu alloy permeation properties: preliminary results*

Using an apparatus and procedure that have been described previously [40], the permeability of a 14 μm thick $Pd_{83}Ag_2Au_{15}$/0.1μmPSS disc (modified with ZrO_2) ternary alloy membrane was compared to that of a similarly prepared pure Pd membrane. At T = 673 K and ΔP = 50 kPa, the alloy membrane displayed pure H_2 permeability of 1.3×10^{-8} mol m^{-1} s^{-1} Pa$^{-0.5}$, slightly higher than that of the pure Pd sample, 1.2×10^{-8} mol m^{-1} s^{-1} Pa$^{-0.5}$. Both membranes had H_2/N_2 ideal selectivity >10,000. After 24 h of exposure to 100 ppm H_2S/H_2 at 673 K, the alloy membrane retained 32% of its initial permeability, while the pure Pd membrane retained only 15%. These preliminary results provide a link between improved permeability performance in the presence of H_2S and the resistance to bulk sulfide formation imparted by the minor alloy components.

4. Conclusions

$Pd_{83}Ag_2Au_{15}$ and $Pd_{74}Ag_{14}Au_{12}$ alloys, synthesized by sequential electroless plating, and a Pd foil reference were treated with 1000 ppm H_2S in H_2 at 623 K for 3 and 30 h. As expected, the Pd foil reacted with H_2S to form a bulk Pd_4S corrosion product within the first 3 h of H_2S exposure. In contrast, neither PdAgAu alloy displayed evidence of bulk sulfide development upon post-exposure examination by XRD, EDS, SEM and X-ray mapping. Local sulfur contamination at the surfaces of the ternary alloys and Pd foil was studied by XPS depth profiling. Consistent with the results of bulk characterization, depth profiles of the H_2S-exposed Pd reference samples show significant concentrations of S (~10 at% in the 3-h sample) throughout the 40 nm etch depth. In contrast, the PdAgAu alloys' sulfur profiles displayed only small S signals at the top-surface (etch time = 0), which disappeared before the etch depth reached ~ 10 nm, even after 30 h of H_2S exposure. The depth profile experiments also revealed significant co-segregation of Ag and Au to the H_2S-exposed alloy surfaces. Preferential location of Au at the alloy surface is likely related to its resistance to bulk sulfidation by H_2S. In a preliminary permeation test, a $Pd_{83}Ag_2Au_{15}$ alloy delivered H_2 fluxes comparable to those of pure Pd, and a residual permeability of 32% in 100 ppm H_2S/H_2 mixed gas experiments at 673 K after 24 h of exposure.

Our work illustrates the resistance of PdAgAu alloys to bulk corrosion by H_2S. It suggests that fabrication of a ternary alloy membrane based on the high-permeability PdAg binary, but with an Au component specifically for H_2S tolerance, could be an effective strategy for improving the membrane performance in extreme environments.

Acknowledgments

The authors wish to acknowledge the financial support received from UNL, ANPCyT, and the NSF-CONICET Program. Thanks are given to Elsa Grimaldi for the English language editing. The authors also wish to acknowledge the National Science Foundation for its support of research on Pd-alloys for hydrogen separation at Carnegie Mellon (CBET 1033804).

REFERENCES

[1] Barbieri G, Brunetti A, Granato T, Bernardo P, Drioli E. Engineering evaluations of a catalytic membrane reactor for the water gas shift reaction. Ind Eng Chem Res 2005;44:7676–83.
[2] Criscuoli A, Basile A, Drioli E. An analysis of the performance of membrane reactors for the water–gas shift reaction using gas feed mixtures. Catal Today 2000;56:53–64.
[3] Kikuchi E. Membrane reactor application to hydrogen production. Catal Today 2000;56:97–101.
[4] Elkina IB, Meldon JH. Hydrogen transport in palladium membranes. Desalination 2002;147:445–8.
[5] Mundschau MV, Xie X, Evenson CR, Sammells AF. Dense inorganic membranes for production of hydrogen from methane and coal with carbon dioxide sequestration. Catal Today 2006;118:12–23.
[6] Thoen PM, Roa F, Way JD. High flux palladium–copper composite membrane for hydrogen separations. Desalination 2006;193:224–9.
[7] O'Brien CP, Gellman AJ, Morreale BD, Miller JB. The hydrogen permeability of Pd_4S. J Membr Sci 2011;371:263–7.
[8] Morreale BD, Howard BH, Iyoha O, Enick RM, Ling C, Sholl DS. Experimental and computational prediction of the hydrogen transport properties of Pd_4S. Ind Eng Chem Res 2007;46:6313–9.

[9] Morreale BD. The iInfluence of H_2S on Palladium and Palladium–Copper aAlloy mMembranes. Chemical Engineering, vol. Doctor of Philosophy, University of Pittsburgh (2006).
[10] McKinley DL. Metal alloy for hydrogen separation and purification. US Patent 3,350,845 (1967).
[11] Kamakoti P, Morreale BD, Ciocco MV, Howard BH, Killmeyer RP, Cugini AV, et al. Prediction of hydrogen flux through sulfur-tolerant binary alloy membranes. Science 2005;307:569–73.
[12] Iyoha O, Enick R, Killmeyer R, Howard B, Ciocco M, Morreale B. H_2 production from simulated coal syngas containing H_2S in multi-tubular Pd and 80wt% Pd–20 wt% Cu membrane reactors at 1173 K. J Membr Sci 2007;306:103–15.
[13] Iyoha O, Enick R, Killmeyer R, Morreale B. The influence of hydrogen sulfide to-hydrogen partial pressure ratio on the sulfidization of Pd and 70 mol% Pd–Cu membranes. J Membr Sci 2007;305:77–92.
[14] Chen C-H, Ma YH. The effect of H_2S on the performance of Pd and Pd/Au composite membrane. J Membr Sci 2010;362:535–44.
[15] Gade SK, DeVoss SJ, Coulter KE, Paglieri SN, Alptekin GO, Way JD. Palladium–gold membranes in mixed gas streams with hydrogen sulfide: effect of alloy content and fabrication technique. J Membr Sci 2011;378:35–41.
[16] O'Brien CP, Howard BH, Miller JB, Morreale BD, Gellman AJ. Inhibition of hydrogen transport through Pd and $Pd_{47}Cu_{53}$ membranes by H_2S at 350 °C. J Membr Sci 2010;349:380–4.
[17] Kulprathipanja A, Alptekin G, Falconer J, Way JD. Pd and Pd–Cu membranes: inhibition of H_2 permeation by H_2S. J Membr Sci 2005;254:49–62.
[18] Gryaznov V. Metal-containing membranes for the production of ultrapure hydrogen and the recovery of hydrogen isotopes. Sep Purif Methods 2000;29:171–87.
[19] Sonwane CG, Wilcox J, Ma YH. Achieving optimum hydrogen permeability in PdAg and PdAu alloys. J Chem Phys 2006;125: 184714–23.
[20] Sonwane CG, Wilcox J, Ma YH. Solubility of hydrogen in PdAg and PdAu binary alloys using density functional theory. J Phys Chem B 2006;110:24549–58.
[21] Gade SK, Payzant EA, Park HJ, Thoen PM, Way JD. The effects of fabrication and annealing on the structure and hydrogen permeation of Pd–Au binary alloy membranes. J Membr Sci 2009;340:227–33.
[22] Ma YH, Akis BC, Ayturk ME, Guazzone F, Enqwall EE, Mardilovich IP. Characterization of intermetallic diffusion barrier and alloy formation for Pd/Cu and Pd/Ag porous stainless steel composite membranes. Ind Eng Chem Res 2004;43:2936–45.
[23] Bosko LM, Miller JB, Lombardo EA, Gellman A, Cornaglia LM. Surface characterization of Pd–Ag composite membranes after annealing at various temperatures. J Membr Sci 2011; 369:267–76.
[24] Ayturk ME, Payzant EA, Speakman SA, Ma YH. Isothermal nucleation and growth kinetics of Pd/Ag alloy phase via in situ time-resolved high-temperature X-ray diffraction (HTXRD) analysis. J Membr Sci 2008;316:97–111.
[25] Bosko LM, Lombardo EA, Cornaglia LM. The effect of electroless plating time on the morphology, alloy formation and H_2 transport properties of PdAg composite membranes. Int J Hydrogen Energy 2011;36:4068–78.
[26] Shi L, Goldbach A, Zeng G, Xu H. Preparation and performance of thin-layered PdAu/ceramic composite membranes. Int J Hydrogen Energy 2010;35:4201–8.
[27] Ahmed S, Lee SHD, Papadias DD. Analysis of trace impurities in hydrogen: enrichment of impurities using a H2 selective permeation membrane. Int J Hydrogen Energy 2010;35: 12480–90.
[28] Coulter KE, Way JD, Gade SK, Chaudhari S, Alptekin GO, DeVoss SJ, et al. Sulfur tolerant PdAu and PdAuPt alloy hydrogen separation membranes. J Membr Sci 2012;405-406: 11–9.
[29] Ayturk ME, Ma YH. Electroless Pd and Ag deposition kinetics of the composite Pd and Pd/Ag membranes synthesized from agitated plating baths. J Membr Sci 2009;330:233–45.
[30] Bhandari R, Ma YH. Pd–Ag membrane synthesis: the electroless and electro-plating conditions and their effect on the deposits morphology. J Membr Sci 2009;334:50–63.
[31] Swartzfager DG, Ziemecki SB, Kelley MJ. Differential sputtering and surface segregation: the role of enhanced diffusion. J Vacuum Sci Technol 1981;19:185–91.
[32] Piccolo L, Piednoir A, Bertolini J. Pd–Au single-crystal surfaces: segregation properties and catalytic activity in the selective hydrogenation of 1,3-butadiene. Surf Sci 2005;592: 169–81.
[33] Yi C-W, Luo K, Wei T, Goodman DW. The composition and structure of Pd–Au surfaces. J Phys Chem B 2005;109: 18535–40.
[34] Li Z, Furlong O, Calaza F, Burkholder L, Poon HC, Saldin D, et al. Surface segregation of gold for Au/Pd (1 1 1) alloys measured by low-energy electron diffraction and low-energy ion scattering. Surf Sci 2008;602:1084–91.
[35] Liu D, Lian JS, Jiang Q. Surface energy and electronic structures of Ag quasicrystal clusters. J Phys Chem C 2009; 113:1168–70.
[36] Ding Y, Fan F, Tian Z, Wang ZL. Atomic structure of Au–Pd bimetallic alloyed nanoparticles. J Am Chem Soc 2012;132: 12480–6.
[37] Barton MD. The Ag–Au–S system. Econ Geol 1980;75:303–16.
[38] Bouchard D, Baleb CW. Measurement of the standard molar Gibbs free energy of formation of Ag_2S using Ag+β-alumina solid electrolyte. J Chem Thermodyn 1995;27:383–90.
[39] Taylor JR. Phase relationships and thermodynamic properties of the Pd–S system. Metall Mat Transact B 1985; 16:143–8.
[40] Tarditi AM, Braun F, Cornaglia LM. Novel PdAgCu ternary alloy: hydrogen permeation and surface properties. Appl Surf Sci 2011;257:6626–35.